Applications and Applied Mathematics: An International Journal (AAM)

Volume 16 | Issue 1 Article 30

6-2021

Theoretical Study of Mach number and Compressibility Effect on the Slender Airfoils

Abrar Hoque
Military Institute of Science and Technology

Masudar Rahman
Bangladesh Army University of Engineering and Technology

Ashabul Hoque
University of Rajshahi

Available at
http://pvamu.edu/aam
Appl. Appl. Math.
ISSN: 1932-9466

Applications and Applied Mathematics:
An International Journal
(AAM)

Vol. 16, Issue 1 (June 2021), pp. 549 – 1xxx

Theoretical Study of Mach number and Compressibility Effect on the Slender Airfoils

[1]Abrar Hoque, [2]Masudar Rahman and [3*]Ashabul Hoque

[1]Department of Aeronautical Engineering
Military Institute of Science and Technology
Dhaka, Bangladesh
abrarrhythm97@gmail.com

[2]Department of Mathematics
Bangladesh Army University of Engineering and Technology
Qadirabad, Bangladesh
masudarmath@gmail.com

[3]Department of Mathematics
University of Rajshahi
Rajshahi-6205, Bangladesh
ashabulh@yahoo.com

[*]Corresponding author

Received: November 23, 2020; Accepted: April 6, 2021

Abstract

Theoretical development of the velocity potential equation for compressible flow and its various consequences has been presented. The geometrical interpretation of potential equation and conformal mapping technique are discussed where the mappings link the flow around a circular cylinder of a slender airfoil. The lift and drag coefficients are determined for the slender airfoils based on the Mach number and compressibility effects. The calculated lift coefficients show that with the increasing of attack angle it increases linearly and a higher lift coefficient is found for a smaller Mach number for any certain attack angle. Similarly, the drag profiles are determined which are exponentially decreased with the increasing of Mach number for any fixed attack angle. The calculated and experimental data on the lift and drag coefficients over the slender airfoil surface are compared and found in good agreement.

Keywords: Slender airfoils; Conformal mapping; Mach number; Attack angle; Supersonic flow; Lift coefficient; Drag coefficient

MSC 2010 No.: 74F05, 97K80, 76F65

Nomenclature

a	= speed of sound;	l	= length of chord;
c	= constant;	M	= Mach number;
C	= curve;	P	= pressure;
C_d	= drag coefficient;	u,v	= velocity components;
C_l	= lift coefficient;	w	= complex function;
C_p	= pressure coefficient;	z	= complex number;
d	= thickness of chord;	α	= angle of attack;
F_l	= lift force;	ρ	= air density;
F_d	= drag coefficient;	∞	= free stream;

1. Introduction

When an aircraft flies through the atmosphere, the air molecules nearby the aircraft are troubled and move around the aircraft. If the aircraft passes at a low speed, (< 250 mph) the density of air remains constant. But for the higher speed of an aircraft, some of the energy of the aircraft converts to compressing the air into moisture or liquid and locally altering the density of the air. This compressibility effect changes the amount of resulting force on the aircraft. The characteristics of compressible flow mainly depend on the Mach number. A compressible flow can be classified into three types, namely subsonic, supersonic and hypersonic based on the Mach number (Rathakrishnan, 2013). For a supersonic aircraft, it may be suitable to choose the most effective supersonic Mach number as its cruise Mach number (Liebhardt et al., 2017). Up to date, researchers in aerodynamic have done massive work dedicated to the control of flow separation in order to increase the aerodynamic performance of flying vehicles. So, understanding the physics of aerodynamic characteristics has a huge impact on the airfoils.

Some studies of compressibility effects on aircraft flying have been performed in the past (Shukla et al. 2019; Shi et al. 2019; Wang and Zha 2019; Colera and Perez-Saborid, 2017; Abdullah et al. 2017; Filiphone, 2007; Chen et al. 1990). Among them, Colera and Perez-Saborid (2017) used a numerical technique to calculate the compressible, subsonic, and unsteady flow based on the time domain those are passed an aerodynamic airfoil. They observed that the results for the particular case of a rigid airfoil showed excellent agreement with those reported by other authors, whereas results in the case of the flexible airfoil were not well-known. Shukla et al. (2019) solved the partial differential equations using non-similar transformations, which were converted into ordinary differential equations. Using the linearized equation for compressible fluid motion, solutions to the flow around any thin symmetric body at zero lift could be found by Puckett (1946), Chen et al. (1990) investigated the influence of Mach number on the stability of a plane supersonic wake and they found the growth rate of stabilizing at a Mach number of 3 which was 60% that of an incompressible wake. Jones and Platzer (1998) presented similar destabilizing effects for both increasing airfoil thickness and increasing Mach number. Courtney et al. (2014) performed the test for supersonic flow at a low air density of 0.9293 kg/m3 and a high air density of 1.1526 kg/m3 and the drag coefficient decreased as Mach number increased

which was expected. Abdullah et al. (2017) investigated the effect of angle of attack on the lifts and drags for airfoils and they observed that the difference in pressure across the asymmetrical airfoils produced higher lift than that across the symmetrical airfoils at a given angle of attack.

On the other hand, many studies have measured aerodynamic characteristics including Mach number effects for standards airfoils. Filippone (2007) showed that a cruise Mach number reasonably lower than the nominal Mach number aided in conserving a significant amount of fuel. Ahmed et al. (2013) used the simulation technique to investigate the aerodynamic significances of simple flapped NACA 0012 airfoil in terms of different flap angles and Mach numbers. They found that the lift coefficient increased with the increase of Mach number, whereas the drag coefficient remained somewhat constant. Xu et al. (2020) determined that with the increase of Mach number, lift coefficient decreased when attack angle was below 10^0 and when attack angle exceeded 12^0, higher Mach number corresponded to a higher lift coefficient. Morizawa et al. (2018) showed that thin and cambered airfoils had larger variations in C_l than symmetric airfoils. That is, they showed that C_l at a higher attack angle α had rapidly increased when the M_∞ was low and C_l became larger than that on the symmetric airfoils when M_∞ was higher. Hao and Gao (2019) showed that the triangular flaps could obtain an increase of maximum lift coefficient by 28.42%, which was better than 16.31% of the rectangular flaps. Anyoji et al. (2014) investigated the effect of the Mach number on the lift and drag characteristics of the flat plate model for a constant Reynolds number, where it was varied from 0.09 to 0.61. Zhou et al. (2017) used the flow separation control method which led to the airfoil (NACA4405) maintain a relatively high lift coefficient even at very large angles of attack, where it was not possible for normal airfoils. Sørensen et al. (2018) showed that at the highest Mach number the lowest Reynolds number gave the highest deviation for both lift and drag coefficients. Kim et al. (2019) showed the numerical study on flow separation control which was conducted for a stalled airfoil with a steady-blowing jet. Their result showed good agreements with the data for lift and drag coefficients. There are many parameters like Reynolds number, thickness ratio, Mach number, angle of attack, lift coefficient, drag coefficient, Prandtl's number, etc. Thus, the connections among Mach number, compressibility effect, pressure distribution, attack angle, lift and drag coefficients for slender airfoils are essential to understand in aerodynamics.

The paper is organized as follows. First, mathematical formulations regarding aircraft flying are presented. Second, the physical interpretation of the potential equation for supersonic flow is discussed. Third, the conformal mapping technique is studied to connect the flow around a circular cylinder to the desired slender airfoil. Finally, the performance of the airfoil will be calculated by considering lift and drag coefficients for different angles of attack with corresponding Mach numbers.

2. Theory

2.1. Slender airfoil geometry

A slender airfoil is the cross-sectional shape of a wing of aircraft (Figure 1). The leading edge of the slender airfoil shape is usually rounded, whereas the trailing edge is sharp. The straight line joining the leading and trailing edges through the centers of curvature is called the length of the

chord (l). The thickness of the airfoil is denoted by d. The chord is a straight line normally used to determine airfoil length and the mean camber line represents a curve midway between the upper and lower surfaces which is measured airfoil curvature. The angle of attack is defined between the chord line and the direction of the flight which is denoted by α. The lift force (F_l) is defined as the component of the actual force working normally of the airfoil and when it is worked horizontally to the airfoil is called drag force (F_d) (Figure 1). The resultant force F_R, generated when fluid flows through the airfoil, can be decomposed into the lift force F_l perpendicular to the flow direction and the drag force F_d parallel to the flow direction. The lift coefficient (C_l) and drag coefficient (C_d) are the two most important parameters are formulated in section 2.5.

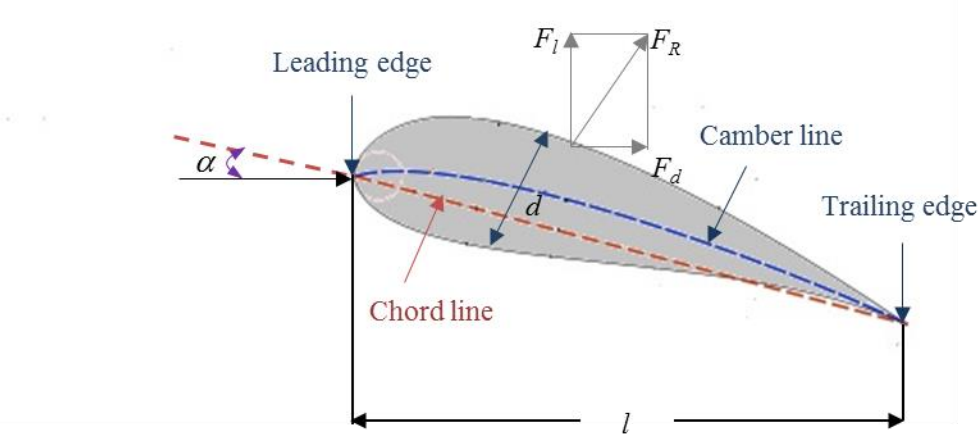

Figure 1. Schematic representation of slender airfoil and its geometry parameters

2.2. Governing equation

To obtain the potential equation for supersonic flow, consider the continuity and Bernoulli's equations, respectively for compressible flow in the following form:

$$a^{-2}\frac{\partial P}{\partial t}+a^{-2}\frac{\partial \phi}{\partial x_i}\frac{\partial P}{\partial x_i}+\frac{\partial^2 \phi}{\partial x_i \partial x_i}=0, \tag{1}$$

$$\frac{\partial \phi}{\partial t}+\frac{1}{2}\frac{\partial \phi}{\partial x_j}\frac{\partial \phi}{\partial x_j}+P+F=C(t), \tag{2}$$

where $dP=(a^2/\rho)d\rho$ is an isentropic change, a represents the speed of sound, ρ is defined as the density of air and $\partial\rho/\partial t$ and $\partial\rho/\partial x_i$ are replaced by $\rho a^{-2}\partial P/\partial t$ and $\rho a^{-2}\partial P/\partial x_i$, respectively. Equations (1) and (2) provide two combined nonlinear equations for P and ϕ. However, to solve these nonlinear equations, the numerical method is necessary.

Consider the steady compressible flow and neglecting the volume body forces (F) and we eliminate P from Equations (1) and (2) and obtain the consequential equation to the form:

$$a^{-2}\frac{\partial\phi}{\partial x_i}\frac{\partial\phi}{\partial x_j}\frac{\partial^2\phi}{\partial x_i\partial x_j}=\frac{\partial^2\phi}{\partial x_i\partial x_i}, \tag{3}$$

Equation (3) is known as the nonlinear partial differential equation for the velocity potential.

Consider slender airfoil ($d/l=\varepsilon<<1$), where *d* and *l* represent thickness and length of an airfoil (Figure 1). The perturbation velocity potential contains a free stream flow and a small fluctuation potential. Mathematically, it can be expressed as

$$\phi=U_\infty x+\varphi, \tag{4}$$

where U_∞ is the free stream velocity in the *x*-direction and φ is the perturbation potential. Further, the perturbation velocities are defined as $u = \partial\varphi/\partial x$ and $v = \partial\varphi/\partial y$ those are small compared to U_∞.

From the energy equation, the expression of a^2 can be found as

$$a^2=a_\infty^2+\frac{\gamma-1}{2}\left(U_\infty^2-\frac{\partial\phi}{\partial x_i}\frac{\partial\phi}{\partial x_i}\right), \tag{5}$$

Multiplying Equation (3) by a^2 on both sides and then inserting the expression of a^2 from Equation (5) into Equation (3), which gives:

$$\frac{\partial\phi}{\partial x_i}\frac{\partial\phi}{\partial x_j}\frac{\partial^2\phi}{\partial x_i\partial x_j}=\left\{a_\infty^2+\frac{\gamma-1}{2}\left(U_\infty^2-\frac{\partial\phi}{\partial x_i}\frac{\partial\phi}{\partial x_i}\right)\right\}\frac{\partial^2\phi}{\partial x_i\partial x_i}\ . \tag{6}$$

Further, the above equation can be written with the support of Equation (4) for 2-dimensional as

$$\begin{aligned}&\frac{\partial}{\partial x}(U_\infty x+\varphi)\frac{\partial}{\partial y}(U_\infty x+\varphi)\frac{\partial^2}{\partial x\partial y}(U_\infty x+\varphi)\\&=\left\{a_\infty^2+\frac{\gamma-1}{2}\left(U_\infty^2-\frac{\partial}{\partial x}(U_\infty x+\varphi)\frac{\partial}{\partial x}(U_\infty x+\varphi)\right)\right\}*\frac{\partial^2}{\partial x^2}(U_\infty x+\varphi).\end{aligned} \tag{7}$$

After some manipulations and algebraic rearranging of Equation (7) and neglecting the terms which are of order $O(\varepsilon^2)$, we obtain a perturbation velocity potential equation as

$$(1-M_\infty^2)\frac{\partial^2\varphi}{\partial x^2}+\frac{\partial^2\varphi}{\partial y^2}=(\gamma+1)M_\infty^2\frac{u}{U_\infty}\frac{\partial^2\varphi}{\partial x^2}+(\gamma-1)M_\infty^2\frac{u}{U_\infty}\frac{\partial^2\varphi}{\partial y^2}+2M_\infty^2\frac{u}{U_\infty}\frac{\partial^2\varphi}{\partial x\partial y}\ , \tag{8}$$

where $M_\infty=U_\infty/a_\infty$ represents the free stream Mach number and it is defined as the ratio of the flow velocity to the speed of sound. Further, although the left-hand side of Equation (8) is linear,

the right-hand-side is nonlinear. Also the right-hand side will vanish for the limit $\varepsilon \to 0$, since every term comprises a factor of order $O(\varepsilon)$. Other way, the right-hand side of Equation (8) will also vanish for $\frac{u}{U_\infty} << 1$. Following any of these hypotheses, Equation (8) can be written as

$$(1-M_\infty^2)\frac{\partial^2\varphi}{\partial x^2}+\frac{\partial^2\varphi}{\partial y^2}=0\ . \tag{9}$$

which is applicable for both subsonic and supersonic flows. For $M_\infty < 1$, Equation (9) is elliptic; whereas when $M_\infty > 1$ for supersonic flow, Equation (9) develops a hyperbolic differential equation. In the present study, we are interested to find a solution of Equation (9) for supersonic flow and put on this solution to determine the supersonic airfoil characteristics.

2.3. Physical interpretation of Equation (9) for $M_\infty > 1$

First. we transform Equation (9) into the following form:

$$\frac{\partial^2\varphi}{\partial x^2}=\frac{1}{c^2}\frac{\partial^2\varphi}{\partial y^2}, \tag{10}$$

where $c^2=(M_\infty^2-1)$ is constant. Defining $u_1=\partial\varphi/\partial x$ and $u_2=\partial\varphi/\partial y$ the equivalent first order set of equations become:

$$L_2=\frac{\partial u_1}{\partial x}-\frac{1}{c^2}\frac{\partial u_2}{\partial y}=0 \text{ and } L_1=\frac{\partial u_1}{\partial y}-\frac{\partial u_2}{\partial x}=0\,. \tag{11}$$

Now L_1 and L_2 provide two partial differential equations in terms of u_1 and u_2 as

$$L=L_1+\lambda L_2=(\frac{\partial u_1}{\partial y}+\lambda\frac{\partial u_1}{\partial x})-(\frac{\partial u_2}{\partial x}+\frac{\lambda}{c^2}\frac{\partial u_2}{\partial y})=0\ . \tag{12}$$

The terms in the first parentheses of Equation (12) can be written as total derivative du_1/dy if $\lambda=dx/dy$. Similarly, the terms in the second parentheses are total derivative du_2/dy if $c^2/\lambda=dx/dy$. Both statements will be correct if dx/dy have the same value, i.e.,

$$\frac{dx}{dy}=\lambda=\frac{c^2}{\lambda}, \tag{13}$$

which leads to:

$$\lambda=\pm c. \tag{14}$$

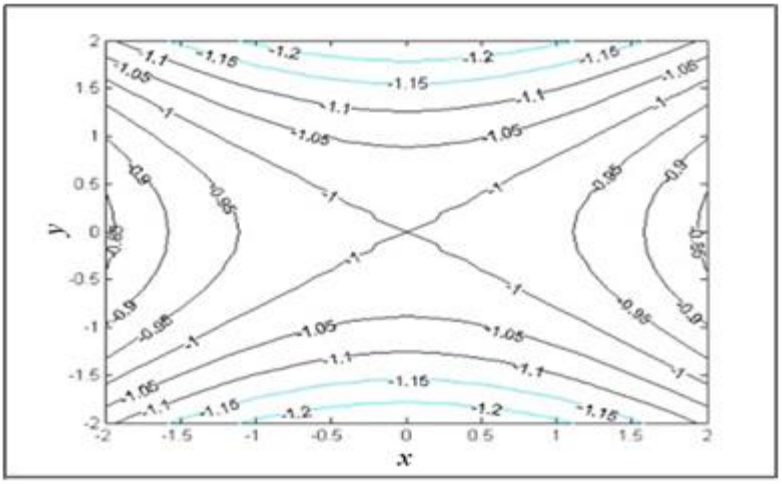

Figure 2. Graphical representation of potential equation for supersonic flow ($M_\infty > 1$)

Since the roots are real and distinct, so Equation (9) represents hyperbolic and its graph is given in Figure (2). Geometrically speaking, the equation shows family of integral surfaces in (x, y) space.

2.4. Analytical solution of Equation (9)

Now it is our intention to solve Equation (9) in order to get the pressure profile along the surface of a slender airfoil as well as lift and drag coefficients and we will restrict to our consideration in the case of supersonic flow. For supersonic flow $(M_\infty > 1)$, Equation (9) reduces to the following wave equation:

$$\frac{\partial^2 \varphi}{\partial y^2} = (M_\infty^2 - 1)\frac{\partial^2 \varphi}{\partial x^2} \ . \tag{15}$$

The general solution of Equation (15) can be specified as a sum of two arbitrary functions:

$$\varphi = h(x - cy) + g(x + cy) \ . \tag{16}$$

In supersonic flow, turbulences can only spread out from the left to the right and we must have $g \equiv 0$ above the airfoil and $h \equiv 0$ below (Figure 3). Mathematically, it can be expressed as

$$\left.\begin{aligned} \phi(x, y) &= h(x - cy), \quad y > 0, \\ \phi(x, y) &= g(x + cy), \quad y < 0. \end{aligned}\right\}. \tag{17}$$

Supersonic flow is examined by the fact that the entrances of the flow are uniform along the characteristic lines $x \pm cy = const.$ It is indicated that the linear approximation of the characteristics are all analogous to one another and lie at the Mach angle of the free stream (Figure 3). First, we assume the flow above the upper side of the airfoil:

$$f(x) = f_{upper}(x) \ . \tag{18}$$

Differentiating Equation (17) with respect to *y*, y-directed perturbation velocity component ($y > 0$) is therefore found as

$$v = \frac{\partial \varphi}{\partial y} = -ch'(x, y) \ . \tag{19}$$

We introduce the boundary condition, $\frac{1}{U_\infty}\frac{\partial \varphi}{\partial y} = \frac{df}{dx}$ for $y = 0$ into Equation (19), yields:

$$v(x,0) = U_\infty \frac{df_{upper}}{dx} = -ch'(x,0) \ . \tag{20}$$

Rearranging and integrating Equation (20), which gives:

$$h(x) = -\frac{U_\infty}{c} f_{upper}(x) . \tag{21}$$

And therefore, using Equation (21) into Equation (17) for the velocity potential at the location $y = 0$, we have

$$\varphi(x) = -U_\infty \frac{f_{upper}(x)}{c} \ . \tag{22}$$

Further, Equation (22) can be written in general form for the whole upper half-plane as

$$\varphi(x, y) = -U_\infty \frac{f_{upper}(x - cy)}{c} . \tag{23}$$

Similarly, we can derive the velocity potential for the lower half-plane as

$$\varphi(x, y) = -U_\infty \frac{f_{lower}(x + cy)}{c} . \tag{24}$$

Equation (23) and Equation (24) together show the complete solution of potential Equation (15) for supersonic flow.

2.5. Lift and drag coefficients

The resultant aerodynamic force F_R on a slender airfoil can be resolved into a lift force F_l perpendicular to the direction of undisturbed flight and a drag force F_d in the direction of flight (Figure 1). These forces are stated in dimensionless form by defining the coefficients of lift and drag as C_l and C_d, respectively. For the derivation of lift and drag coefficients, we consider a thin, 2-dimensional, symmetric airfoil is positioned in a supersonic flow at a Mach number

where the attack angle is α. For a thin camber airfoil in supersonic flow, the pressure coefficient (C_p) is found on the upper side of the airfoil with the help of Equation (22) as

$$C_{pupper} = -\frac{2}{U_\infty}\frac{\partial \phi}{\partial x} = \frac{2}{c}\frac{df_{upper}}{dx}. \tag{25}$$

Similarly, for the lower side of the airfoil, it can be found as

$$C_{plower} = -\frac{2}{U_\infty}\frac{\partial \varphi}{\partial x} = -\frac{2}{c}\frac{df_{lower}}{dx}. \tag{26}$$

The lift on both surfaces will be twice the integral of the pressure (C_p) over the airfoil surface. According to the definition of the lift coefficient, the linearized theory gives the expression as

$$C_l = \frac{1}{l}\oint C_p dx = \frac{1}{l}\int_0^l (C_{plower} - C_{pupper})dx. \tag{27}$$

Now inserting expressions for C_{pupper} and C_{plower}, the integration yields the total lift coefficient at an angle of attack α as

$$C_l = \frac{4\alpha}{\sqrt{M_\infty^2 - 1}}, \tag{28}$$

where $f_{upper}(l) = f_{lower}(l) = -\frac{\alpha l}{2}$ and $f_{upper}(0) = f_{lower}(0) = \frac{\alpha l}{2}$ (as shown in Figure 3(a)).

In the same way, the analogous calculation furnishes the drag coefficient as

$$C_d = \frac{2}{cl}\int_0^l \left[\left(\frac{df_{lower}}{dx}\right)^2 + \left(\frac{df_{upper}}{dx}\right)^2\right]dx. \tag{29}$$

After integrating and using the functional values of $f_{lower}(x)$ and $f_{upper}(x)$ at $x = 0$ and $x = l$, which can be found from Figure 3(a)

$$C_d = \frac{4\alpha^2}{\sqrt{M_\infty^2 - 1}}. \tag{30}$$

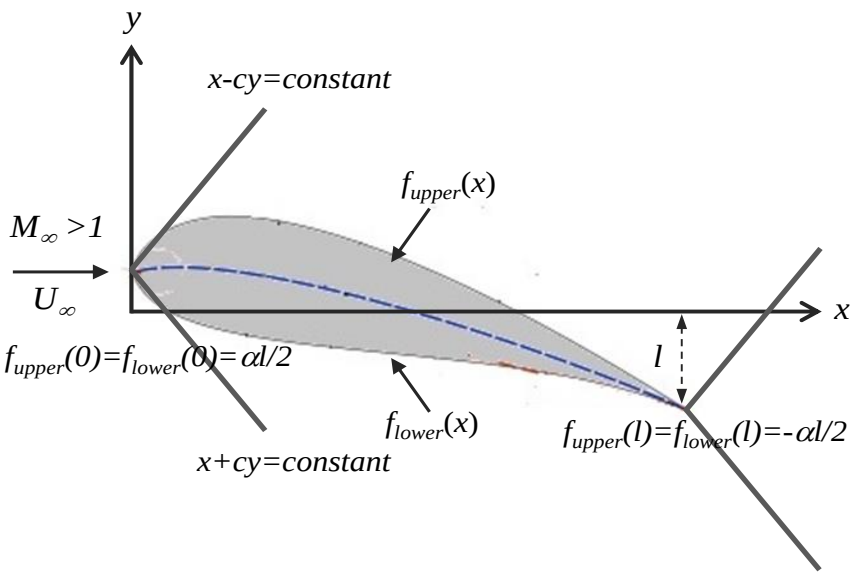

(a)

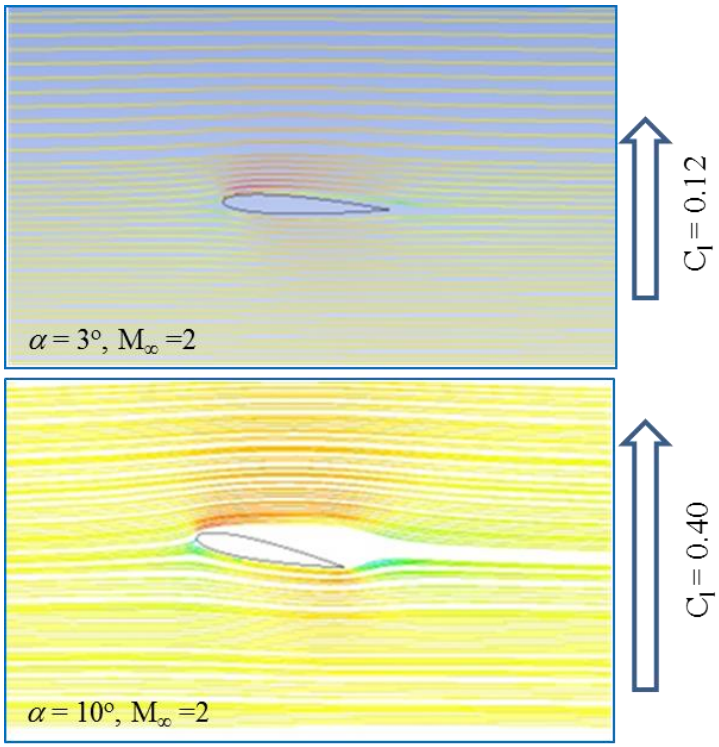

(b)

Figure 3. (a) Sketch of supersonic flow past a slender past airfoil and (b) computational flow field of streamlines around the slender airfoil for $\alpha = 3^o$ and $\alpha = 10^o$ at $M_\infty = 2$

The physical appearance of a finite wing at supersonic speeds follows the identical functional variations with the attack angle, specifically C_l is related to α and C_d is proportional to α^2. Although there are many parameters like Reynolds number, Mach number, angle of attack,

Prandtl's number, etc are directly related to the airfoil. But here the performance of the airfoil was calculated only for considering lift and drag coefficients with different attack angles and Mach numbers. The rounded leading edge causes the airflow over the thin airfoils to become more susceptible to flow separation, and thus leads to higher lift and drag coefficients for higher attack angles as can be seen in Figure 3(b). Similar results were concluded by Ahmed et al. (2013). They also showed that the lift coefficient (C_l) and drag coefficient (C_d) were increased with the increase of different flap angles for any certain Mach number (M_∞) of plain flapped NACA 0012 airfoil.

2.6. Conformal mapping for generating airfoil shape

With the aid of conformal mapping, the flow past a circular cylinder is possible to transform the flow past an airfoil shape. By the conformal mapping function, the region outside the circular cylinder in the *z*-plane is mapped onto the region outside the cylinder in the *w*-plane. The mapping Figure 4(b) in the *w*-plane will be a general airfoil with both camber and thickness if the circle in the *z*-plane is changed in both *x* and *y* directions. If we plot a circle whose center (x_0, y_0) is not zero, it gives typical airfoils. Such airfoils are produced from the well-known Joukowsky transformation.

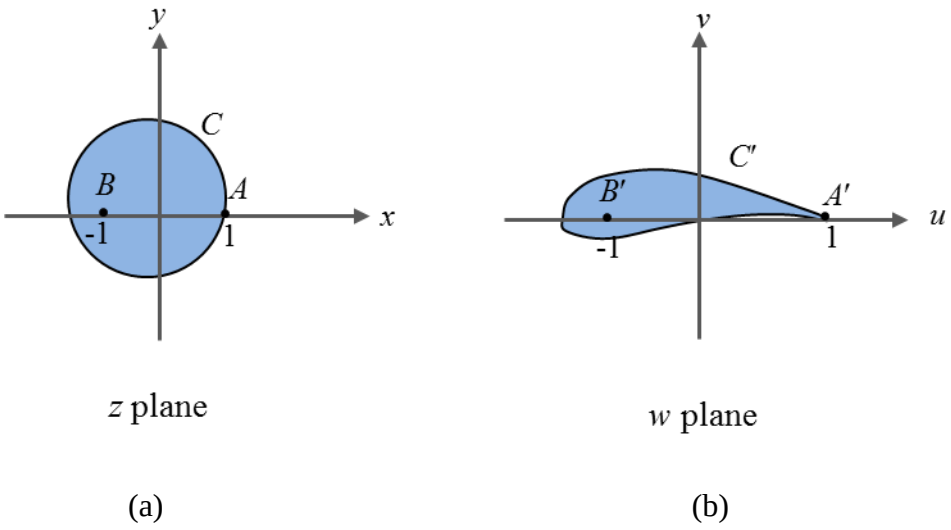

Figure 4. A conformal mapping of (a) a circular cylinder onto (b) a slender airfoil

The Joukowsky transformation is used because it has the property of transforming circles in the *z* plane into shapes that resemble airfoils in the *w* plane as

$$w = f(z) = \frac{1}{2}\left(z + \frac{1}{z}\right). \tag{31}$$

Now differentiating Equation (31) with respect to *z* which gives in bellow

$$\frac{dw}{dz} = \frac{1}{2}\left(1 - \frac{1}{z^2}\right). \tag{32}$$

For the critical point, we set up $dw/dz = 0$ which gives $z = \pm 1$. The point $z = -1$ is usually mapped inside the slender airfoil, so it is, therefore, no concern to us. So, the trailing edge angle is zero, a standard property of the Joukowski mapping, that is already evident from the mapping of the circle of radius 1 to a slit and it gives also the sharp tail at $w = 1$ for $z = 1$ (Figure 4(b)). If C does not entirely enclose the circle $|z| = 1$ (as shown in Figure 4(a)), image C' will not entirely enclose the image of $|z| = 1$. Instead, C' will only enclose that portion of the slot which corresponds to the part of $|z| = 1$ inside C. The shape of C' in the w-plane is, therefore, unsymmetrical which is known as cambered airfoil shown in Figure 4(b). The x-intercepts of the circle in the z-plane develop the leading and trailing edges of the airfoil in the w-plane.

3. Results

The curves show the variation of lift (C_l) and drag (C_d) coefficients with the different attack angles (α) and Mach numbers (M_∞) in Figure 5. Although the flow having Mach number greater than 0.3 is treated as compressible flow, but in the present study, if it is in between 0.3 to 1, the flow is said to be transonic which is regarded as complex effects. So, our investigation is restricted only to supersonic flow ($M_\infty > 1$) where the flow becomes also strongly compressible.

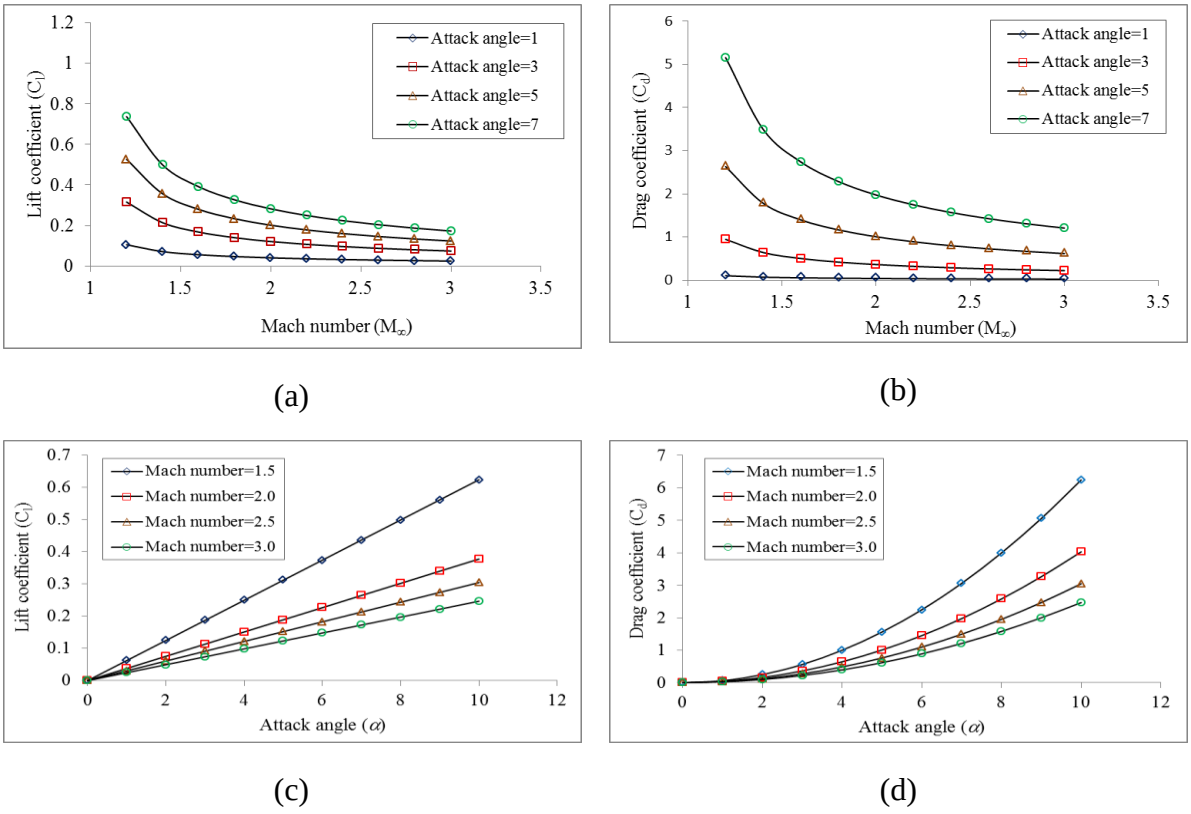

Figure 5. Profiles of lift and drag coefficients with different Mach numbers and attack angles: (a) C_l vs M_∞; (b) C_d vs M_∞; (c) C_l vs α and (d) C_d vs α

In Figure 5(a), the variation of lift coefficient (C_l) with Mach number is presented with different choices of attack angles. It can be seen that the lift coefficient is decreased with the increase of the Mach number and a higher lift coefficient is found for higher attack angles at any Mach number. A similar result can be observed for the drag coefficient in Figure 5(b). In Figure 5(c), the lift coefficient is also plotted against the attack angle with different choices of Mach numbers and the lift curves show the linear with the increasing of Mach number. In addition, the drag coefficient is exponentially increased with the increase of attack angle, and a higher drag coefficient is obtained for lower Mach number at any attack angle (Figure 5(d)).

Lift and drag coefficients at different Mach numbers ($0.2 \le M_\infty \le 0.9$) were measured against the attack angles for symmetric and cambered airfoils (Morizawa et al. 2018). Although our results of C_d are found a similar tendency to their results, however, lift coefficients (C_l) are observed in different patterns. Xu et al. (2020) demonstrated that the lift coefficient was varied linearly proportional to the attack angle for a section (C_l < 1.0) at Mach number from 0.65 to 0.75, but it was contrary when the lift coefficient was higher than 1.0. The present study for lift coefficient also shows linear variations and it was restricted only for supersonic flow (M_∞ > 1).

Equations (28) and (30) are also plotted in three dimensions. These are shown in Figure 6. It can be seen that lift and drag coefficients both are increasing with the increase of attack angle for a certain Mach number. Kuzmin (2015) determined a discontinuous dependence of the lift coefficient on the angle of attack ($-0.6\text{deg} \le \alpha \le 0$) and Mach number ($0.85 \le M_\infty \le 0.86$), in which the lift coefficient exhibited a high sensitivity to small perturbations.

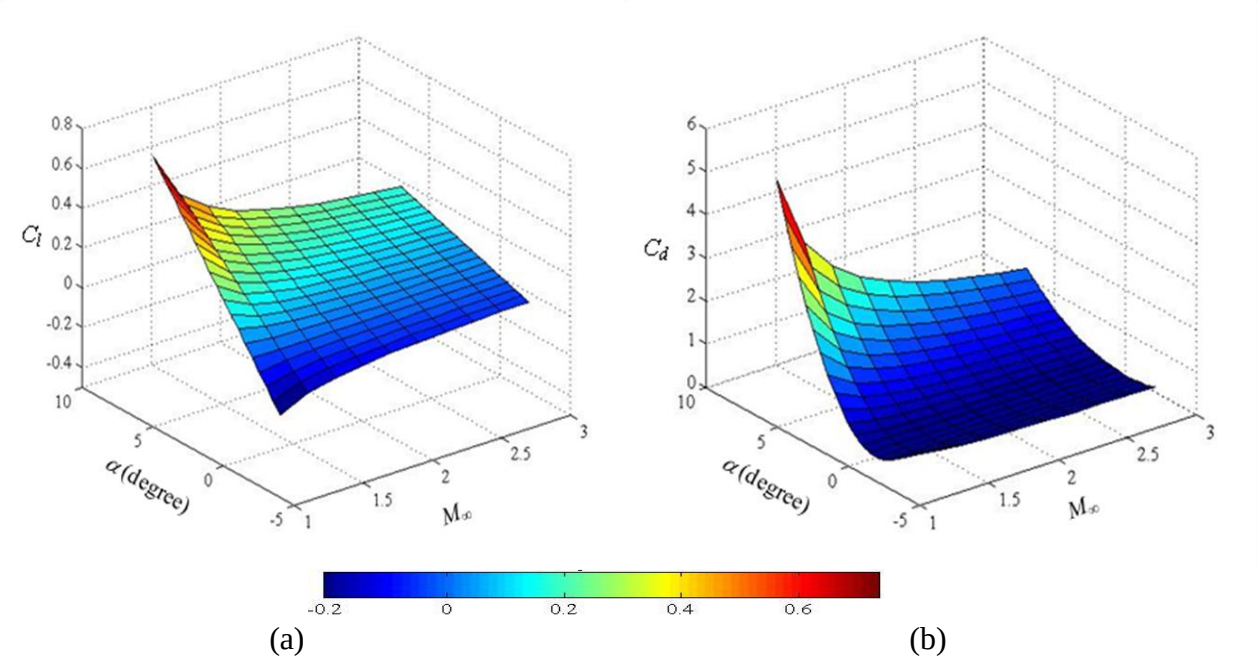

Figure 6. Showing the lift coefficient C_l and drag coefficient C_d of the airfoil: (a) the image corresponds to a C_l - α - M_∞ and (b) C_d is a function of M_∞ and the angle of attack α for 3-D

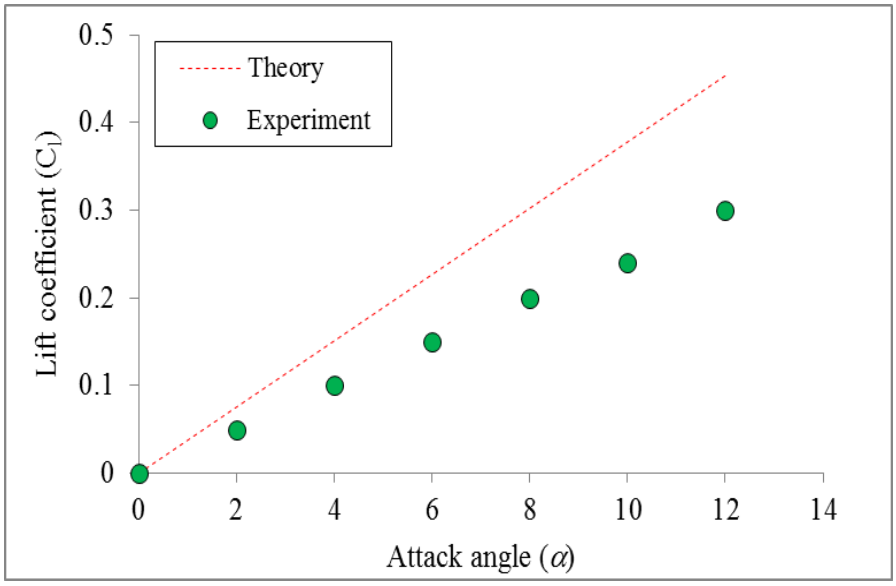

(a)

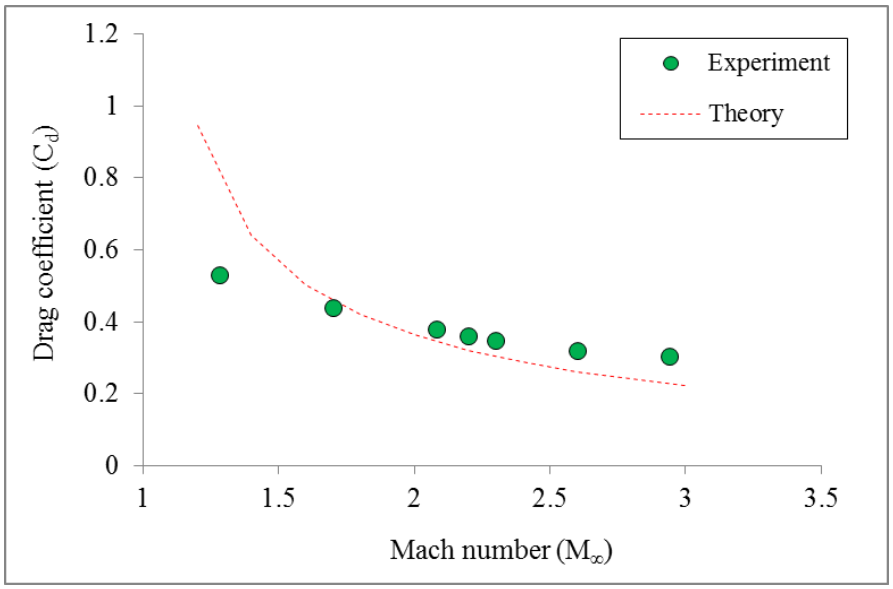

(b)

Figure 7. Comparison of calculated results with the experimental data: (a) lift coefficient vs attack angle for M_∞ =2.0 (Data are taken from Yong, 2019), and (b) drag coefficient vs Mach number for α = 3^o (Experiment conducted by Courtney et al., 2014)

Further, the lift coefficient C_l diagram in Figure 7(a) for supersonic flow with Mach number of 2.0, which is plotted to prove the result consistency between calculated and experimental data, and the agreement is found good, although there is a discrepancy when the attack angle $\alpha > 4$ degrees. The lift coefficient was overestimated at higher attack angles and this overestimation is expected because the flow separates from the leading edge of the airfoil for angles of attack above 4 under the present condition. Again, in Figure 7 (b), under the supersonic flow condition, we have compared the calculated and experimental data of the drag coefficient C_d and the result is usually in good agreement with the experimental results, there are certain differences around M_∞ = 1.3. Anyoji et al. (2014) investigated the effect of the Mach number on aerodynamic characteristics of a flat plate in Mach number up to 0.61, which was almost negligible and their results also showed the lift coefficient might be different with the increased Mach number above the attack angle α = 15 deg.

4. Conclusions

For the aeronautical community, an important application of the most efficient supersonic Mach number was used to determine the lift and drag coefficients. First, we studied the potential equation for supersonic flow. Secondly, we used the technique of conformal mapping to investigate the fluid movement around the cambered airfoils by using the Joukowsky transformation to connect the flow solution for a cylinder to that of an airfoil. The Joukowsky transformation was used because it had the property of transforming circles in the *z* plane into shapes that resemble airfoils in the *w* plane (Benson, 1996). Finally, we were able to successfully map the solution for the inviscid flow around a cylinder to the flow around an airfoil shape using the Joukowsky transformation.

.

This paper also focused on the Mach number and compressibility effects theoretically for the slender airfoil. The investigations of the lift and drag coefficient distributions indicated that the main effect with respect to compressibility originated from the change to the lift and drag distributions, while the attack angle affects similarly on the main parameters. Clearly, the calculated results of the lift and drag coefficients were decreased exponentially with the increase of Mach number, and a higher lift coefficient was obtained for higher attack angles at a certain Mach number. In addition, these results also plotted against the attack angle, where lift and drag coefficients increased linearly and exponentially, respectively at a certain Mach number. Moreover, images of the lift and drag coefficients were also determined in three dimensions those corresponded to C_l - α - M_∞ and C_d - α - M_∞. That is, lift and drag coefficients both were increased with the increasing of attack angle for a certain Mach number. Further, Figure 7 compared the current analytical solution and the experiment in terms of the airfoil's lift and drag coefficients. This result indicated that the present simulation accurately predicted aerodynamic performances of drag coefficient with the Mach number, although the lift coefficient was overestimated at higher angles. This overestimation is expected because the flow separates from the leading edge of the airfoil for angles of attack above 4 under the present condition.

Acknowledgements

The authors would like to thanks the reviewers' comments and suggestions that improved the content of the present paper.

REFERENCES

Abdullah A., Jafri M. N. S. M. and Zulkafli M. F. (2017). Numerical study of military airfoils design for compressible flow, *ARPN* Journal of Engineering and Applied Sciences, Vol. 12, No. 24, pp. 7129-7133.

Ahmed T., Amin M. T., Islam S.M.R. and Ahmed S. (2017). Computational study of flow around a NACA 0012 wing flapped at different flap angles with varying Mach numbers, Global Journal of Researches in Engineering, Vol. 13, No. 4, pp. 5-16.

Anyoji M., Numata D., Nagai H., and Asai K. (2014). Effects of Mach Number and Specific Heat Ratio on Low-Reynolds-Number Airfoil Flows, AIAA, Vol. 53, No. 6, pp. 1640-1654.

Benson T.J. (1996). Interactive educational tool for classical airfoil theory, Cleveland, Ohio: NASA Lewis Research Center, Oct. 30, http://www.grc.nasa.gov/WWW/K-12/airplane/FoilTheory.pdf

Chen J. H., Cantwell B. J. and Mansour N. N. (1990). The effect of Mach number on the stability of a plane supersonic wake, Physics of Fluids, Vol. 2, No. 6, pp. 984-1004.

Courtney E., Courtney A., and Courtney M. (2014). Experimental tests of the proportionality of aerodynamic drag to air density for supersonic projectiles, Proceedings of the 28th International Symposium on Ballistics.

Colera M. and Pérez-Saborid M. (2017). An efficient finite differences method for the computation of compressible, subsonic, unsteady flows past airfoils and panels. Journal of Computational Physics, Vol. 345, pp. 596-617.

Filippone A. (2007). On the benefits of lower Mach number aircraft cruise, The Aeronautical Journal, Vol. 111, pp. 531-542.

Hao L. and Gao Y (2019). Effect of gurney flap geometry on a S809 airfoil; International Journal of Aerospace Engineering, Vol. 2019, pp. 1-8.

Jonesy K. D. and Platzerz M. F. (1998). Airfoil geometry and flow compressibility effects on wing and blade flutter. AIAA Paper No. 98-0517, 36th AIAA Aerospace Sciences Meeting, Reno, Nevada, http://hdl.handle.net/10945/37209.

Kim J., Park Y. M., Lee J., Kim T., Kim M., Lim J. and Jee S. (2019). Numerical investigation of jet angle effect on airfoil stall control. Applied Sciences, Vol. 9.

Kuzmin A. (2015). A sensitivity analysis of transonic flow over J-78 wings. International Journal of Aerospace Engineering ID 579343, 6 pages.

Liebhardt B., K. Lütjens, R. R. Tracy and A. O. Haas (2017). Exploring the prospect of small supersonic airliners-A case study based on the aerion AS2 Jet. *AIAA*. doi.org/10.2514/6.2017-3588.

Morizawa S., Nonomura T., Oyama A., Fujii K. and Obayashio S. (2018). Effect of Mach number on airfoil characteristics at Reynolds number of 3,000, Trans. Japan Soc. Aero. Space Science, Vol. 61, No. 6, pp. 258–267.

Puckett, A.E. (1946). Supersonic wave drag of thin airfoils, Journal of the Aeronautical Sciences, Vol. 13, No. 9, pp. 475-484.

Rathakrishnan E. (2013). *Theoretical Aerodynamics*. Singapore: John Wiley & Sons Singapore Pte. Ltd.

Shi A., Chen J., Dowell E. H. and Wen H. (2019). Approach to determine the most efficient supersonic Mach number, AIAA Journal, Vol. 58, pp. 1402-1406.

Shukla H., Surati H. C., and Timol M.G. (2019). Local Non-Similar Solution of Powell-Eyring Fluid flow over a Vertical Flat Plate, Application and Applied Mathematics, Vol. 14, pp. 973 – 984.

Sørensen N. N., Bertagnolio F., Jost E. and Lutz T. (2018). Aerodynamic effects of compressibility for wind turbines at high tip speeds, IOP Conf. Series: Journal of Physics, Vol. 1037.

Wang Y. and Zha G. (2019). Study of Mach number effect for 2D co-flow jet airfoil at cruise conditions, AIAA Aviation Forum, doi: 10.2514/6.2019-3169.

Xu J., Song W., Hany Z. and Zhao Z. (2020). Effect of Mach number on high-subsonic and low-Reynolds-number flows around airfoils, International Journal of Modern Physics B, Vol. 34, pp. 2040112(1-7).

Yong, W. (2019). Study on Aerodynamic Characteristics of Supersonic Airfoil, Modern Mechanical Engineering, Vol. 9, pp. 13-19.

Zhou Y., Hou L., Huang D. (2017). The effects of Mach number on the flow separation control of airfoil with a small plate near the leading edge, Computers and Fluids, Vol. 156, pp. 274-282.